Structural, Textural, and Electronic Properties of a Nanosized Mesoporous $Zn_xTi_{1-x}O_{2-x}$ Solid Solution Prepared by a Supercritical Drying Route

Yury V. Kolen'ko,*[,†,‡] Kirill A. Kovnir,[‡,§,▽] Anton I. Gavrilov,[‡] Alexei V. Garshev,[‡] Pavel E. Meskin,[∥] Bulat R. Churagulov,[∥] Michel Bouchard,[⊥] Christophe Colbeau-Justin,[⊥] Oleg I. Lebedev,[#,○] Gustaaf Van Tendeloo,[#] and Masahiro Yoshimura[†]

Materials and Structures Laboratory (Center for Materials Design), Tokyo Institute of Technology, 4259 Nagatsuta, Midori-ku, Yokohama 226-8503, Japan, Department of Materials Science, Moscow State University, Moscow 119992, Russia, Max-Planck-Institut für Chemische Physik fester Stoffe, Dresden 01187, Germany, Department of Chemistry, Moscow State University, Moscow 119992, Russia, LIMHP (CNRS, UPR1311), 99 av. J-B Clément, Villetaneuse 93430, France, and EMAT, University of Antwerp, Groenenborgerlaan 171, Antwerpen B-2020, Belgium

Received: June 29, 2005; In Final Form: September 5, 2005

Mesoporous nanosized TiO_2 and $Zn_xTi_{1-x}O_{2-x}$ solid solution having a Zn content below 10 mol % with a particles size between 13 and 17 nm are prepared by a template-free sol-gel method followed by high-temperature supercritical drying in 2-propanol. The structural, textural, and electronic properties of the obtained nanomaterials are methodically investigated by using XRD, SEM, TEM, ED, HREM, EDX, ICP-OES, N_2 adsorption−desorption, Raman spectroscopy, and diffuse reflectance UV−vis spectroscopy. It is shown that the proposed synthesis technique leads to the formation of a $Zn_xTi_{1-x}O_{2-x}$ solid solution based on the anatase crystal structure rather than a two-phase sample. High-resolution electron microscopy and electron diffraction indicate that the distribution of zinc atoms over the anatase structure does not lead to a considerable deformation of the crystal structure.

Introduction

In recent years, the intensive activities in modern material chemistry are devoted to the design and fabrication of nanostructured systems based on titanium dioxide with peculiar physical-chemical properties. The driving force for pursuing research on TiO_2 is the wide range of its applications. Presently, titania and TiO_2-based composites are widely used as white painting materials,[1] beam splitters, optical, antireflection, and corrosion-protective coatings, ceramics,[2] gas sensors,[3] solar cells,[4] electric and electrochromic devices,[5] biocompatible bone implants,[6] etc. Also, TiO_2 plays important role for advanced catalytic applications[7] and, in particular, for photocatalytic purification/disinfection of water and air.[8] Most of the listed applications of titania should possess a number of specific properties such as nanosized particle, crystalline quality, surface state, specific surface area, morphology (e.g., mesoporous), etc. It should be noted that doping the TiO_2 with various metal ions may lead to an enhanced efficiency of such materials. For example, photoinduced charge-carrier separation can be actually favored in such metal/TiO_2 nanocomposites, as proved by the enhancement of photocatalytic[9] and photoelectrochemical[10] performances in combined materials.

Presently, in the literature, the main attention is paid to the investigation of noble metal/TiO_2,[11] alkaline earth/TiO_2 and rare earth/TiO_2,[12] and other M^{n+}-doped titanium dioxide catalytical systems.[13] In the case of photocatalysis, doping with a different metal has a large influence on the charge-carrier recombination time[14] and photoactive transition in the visible light[15] which result in enhanced photodegradation. Moreover, the method of doping leads to different morphological and crystalline properties of the catalyst. Due to these remarkable reasons, modifying TiO_2 by adding some heteroelements is viewed as one of the most important ways to explore novel catalysts.

In this work, we focus on the preparation and investigation of Zn^{2+}-doped TiO_2 nanocomposites. For the synthesis, we used a sol-gel method followed by supercritical drying in 2-propanol. This synthetic method generally allows control of the texture, the chemical, and the morphological properties of the solid and has several advantages compared to other methods, such as impregnation or coprecipitation, which are used to introduce dopants. The advantages of the sol-gel technique are molecular-scale mixing of the components, high purity of the precursor, and homogeneity of the sol-gel products with a high isotropy of physical, morphological, and chemical properties.[16] For supercritical drying, two basic ways are applied presently—high-temperature techniques and various low-temperature methods.[17] It is important to note that powders obtained by the high-temperature technique can be used as catalysts directly after drying without an additional thermal treatment. In addition, the

* To whom correspondence should be addressed. Mailing address: Dr. Yury V. Kolen'ko, R3−20, Center for Materials Design, Materials and Structures Laboratory, Tokyo Institute of Technology, 4259 Nagatsuta, Midori-ku, Yokohama 226-8503, Japan. Tel: +81-(0)45-924-5368. Fax: +81-(0)45-924-5358. E-mail: kolenko@msl.titech.ac.jp.

† Tokyo Institute of Technology.

‡ Department of Materials Science, Moscow State University.

§ Max-Planck-Institut für Chemische Physik fester Stoffe.

∥ Department of Chemistry, Moscow State University.

⊥ LIMHP.

University of Antwerp.

▽ Present address: Department of Inorganic Chemistry, Fritz-Haber-Institut der MPG, D-14195 Berlin, Germany.

○ On leave from the Institute of Crystallography RAS, Moscow 117333, Russia.

10.1021/jp0535341 CCC: $30.25
Published on Web 00/00/0000 PAGE EST: 7

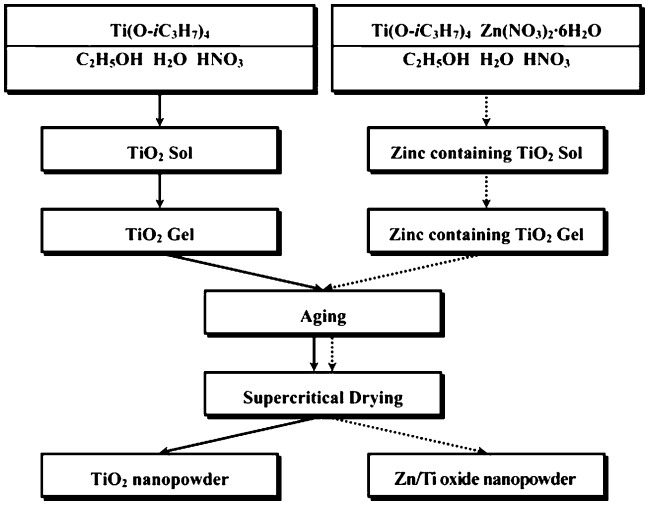

Figure 1. Sol-gel and drying flowchart.

sol-gel method in combination with supercritical drying is a most promising template-free method to prepare materials with a mesoporous structure.[16c]

Here, we report the synthesis together with the structural, textural, and electronic properties of sol-gel-derived mesoporous $Zn_xTi_{1-x}O_{2-x}$ solid solutions converted into powder by supercritical drying in 2-propanol.

Experimental Section

Nanocomposite Preparation. Nanocrystalline titania and Zn/TiO_2 nanocomposites are prepared by a sol-gel method followed by supercritical drying in 2-propanol (shown schematically in Figure 1). The sol-gel preparation of a titania gel is based on the route elaborated by Dagan et al.[18] First, the metal-alkoxide precursor (Ti(O-*i*-$C_3H_7)_4$, Acros, 98%, 18.58 cm^3) is dissolved in absolute ethanol (Prolabo, 99.85%, 51.00 cm^3). The hydrolyzant consisted of distilled water (0.87 cm^3) and 2 mol/L aqueous nitric acid solution (Prolabo, 69%, 2.5 cm^3) diluted in absolute ethanol (15 cm^3). The hydrolyzant is added drop-by-drop to the alkoxide solution at room temperature under continuous stirring (400 rpm).

The zinc-doped titania gels, with a Zn content of 0.1, 0.2, 0.3, 0.5, 1.0, 2.0, 5.0, and 10.0 mol %, are synthesized using mixed precursors prepared by dissolving the calculated stoichiometric amount of zinc nitrate ($Zn(NO_3)_2{\cdot}6H_2O$, Prolabo, 99.9%) in the 51.00 cm^3 absolute ethanol before the addition of Ti(O-*i*-$C_3H_7)_4$.

Within ~30 min a monolithic, transparent, pure, or zinc-containing titania alcogel is obtained. The resulting gel is aged for 12 h at room temperature.

To obtain a powder from the alcogel, we perform drying under supercritical conditions of *i*-C_3H_7OH (T_c = 235.1 °C, P_c = 47.6 bar, ρ_c = 0.273 g/cm^3). When the pore liquid is removed as a gas phase from the interconnected solid gel network under supercritical conditions (critical-point drying method), the network does not collapse and a low-density aerogel is produced. Alcogel is then put into a stainless steel autoclave (volume, 150 cm^3, degree of filling by *i*-C_3H_7OH, 80%). The solvents present in the alcogel (EtOH, H_2O, and *i*-C_3H_7OH) are replaced by an *i*-C_3H_7OH flow of 5 cm^3/min for 1 h at a pressure of 100 bar and a temperature of 300 °C. At the end of the supercritical drying, the autoclave is removed from the furnace and cooled to room temperature.

After supercritical drying, ~5 g of off-white pure titania and a series of Zn/TiO_2 nanocomposites are obtained. To remove most of the organic residues, a thermal treatment of the samples is carried out at 500 °C in an atmosphere of air. The treatment includes a 6 h heating to the final temperature and a 10 h ramp.

Throughout this work, a set of acronyms is used: **0%Zn/TiO_2**, **0.1%Zn/TiO_2**−**10%Zn/TiO_2**. The numbers indicate the mol % of zinc content in the nanocomposites.

Characterization and Property Measurements. Powder X-ray diffraction (XRD) patterns were collected at a Huber G670 Image Plate camera using CuKα1 radiation (λ = 1.540598 Å). The size of the titania crystallites was calculated by means of Scherrer's equation (line-broadening analyses) from the broadening of the 101 XRD reflection for anatase (DRON-3M diffractometer, CuKα radiation, λ = 1.54183 Å, 0.03°/4 s). Room-temperature Raman scattering measurements were carried out on a micro-Raman Jobin Yvon Lab HR800 system with a 487.986 nm Ar^+ ion laser (Coherent) as the excitation light. The scattered light was collected in the backscattering geometry using a liquid nitrogen cooled CCD detector. The morphology was studied by scanning electron microscopy (SEM) using a Leo Supra 50 VP microscope operating at 5 kV with INCA energy + spectrometer for energy-dispersive X-ray spectroscopy (EDX) operating at 20 kV. Electron diffraction (ED) and high-resolution electron microscopy (HREM) investigations were performed using a JEOL 4000 EX microscope operating at 400 kV. The sample for transmission electron microscopy (TEM) was crushed, dispersed in methanol, and deposited on a holey carbon grid. Computer-simulated images for a different defocus and different thickness were obtained using the Crystalkit and MacTempas programs. Diffuse reflection spectra were recorded in a Perkin-Elmer Lambda 35 UV−vis spectrophotometer using a diffuse reflection cell. Chemical analysis was performed by inductively coupled plasma optical emission spectrometer (ICP-OES) methods on a Varian Vista RL spectrometer. All values are the average of at least three replicates. Adsorption−desorption measurements of N_2 at 77 K using a COULTER SA 3100 have been realized to determine the surface area by the multipoint Brunauer−Emmett−Teller method (BET) and the pore size distribution by the Barrett−Joyner−Halenda method (BJH).

Results and Discussion

The phase composition, particle size, specific surface area, pore volume, and band-gap energy of synthesized powders are given in Table 1.

The EDX analysis of the samples **0.2%Zn/TiO_2**, **0.5%Zn/TiO_2**, and **5%Zn/TiO_2** confirms the presence of zinc in the samples. The average atomic percent of the titanium and zinc elements are 36.80% and 0.07% (Zn/Ti ~ 0.19%) for sample **0.2%Zn/TiO_2**, 29.21% and 0.18% (Zn/Ti ~ 0.62%) for sample **0.5%Zn/TiO_2**, and 31.52% and 1.6% (Zn/Ti ~ 5.08%) for sample **5%Zn/TiO_2**; this is in good agreement with the initial molar ratio under sol-gel synthesis. Moreover, according to EDX data, the distribution of Zn in these samples is quite uniform. The ICP-OES analysis of sample **5%Zn/TiO_2** shows that the content of Zn ions in this powder is ~4.81 mol %, which is also in agreement with the EDX results.

According to XRD data (Figure 2), supercritical drying of alcogels in 2-propanol leads in all cases to the formation of nanocrystalline anatase (JCPDS no. 21-1272)—a metastable form of TiO_2, which does not transform to rutile during the removal of most of the organic residues by a thermal treatment at 500 °C for 10 h (Table 1). The particle size of Zn-doped powders slightly decreases from 17 to 13 nm (line-broadening analyses) with the nominal content of zinc increasing as compared to

TABLE 1: Properties of the Nanocrystalline Titania and Zn/TiO_2 Nanocomposites Prepared by a Sol-Gel Method Followed by Supercritical Drying in Isopropanol

	XRD					
reference	phase composition[a]	particles size (nm)	fwhm (cm^{-1}) [b]	BET area (m^2/g)[c]	V_{meso} (cm^3/g)[d]	E_{bg} (eV)[e]
0%Zn/TiO_2	anatase	17	11.26	77	0.38	2.96
0.1%Zn/TiO_2	anatase	14	–	84	0.43	2.96
0.2%Zn/TiO_2	anatase	15	11.47	83	0.42	2.96
0.3%Zn/TiO_2	anatase	15	–	85	0.54	2.97
0.5%Zn/TiO_2	anatase	15	11.82	80	0.50	2.97
1%Zn/TiO_2	anatase	15	–	82	0.51	3.00
2%Zn/TiO_2	anatase	14	–	86	0.53	2.99
5%Zn/TiO_2	anatase	13	12.20	92	0.57	3.00
10%Zn/TiO_2	anatase	13	12.27	94	0.74	3.02

[a] No Zn-containing phases were detected by XRD. [b] Line width of the Raman $E_{g(1)}$ mode. [c] Calculated by BET method. [d] Calculated by BJH method. [e] Band-gap energies calculated by the Kubelka–Munk method.

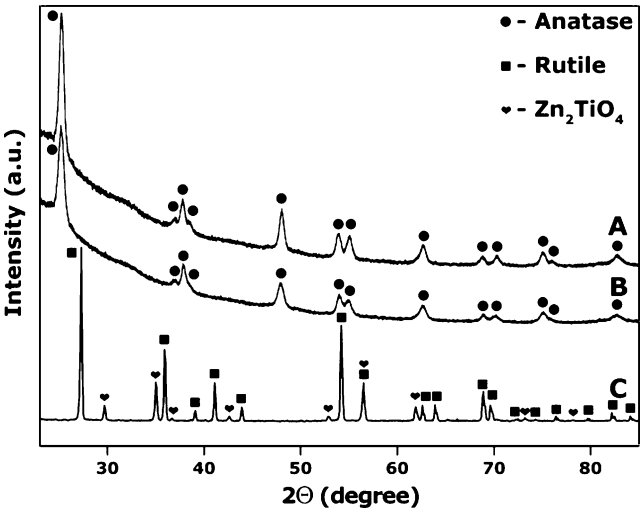

Figure 2. Powder X-ray diffraction patterns of a TiO_2 and Zn/TiO_2 nanocomposites synthesized by the sol-gel method followed by supercritical drying: (A) **0%Zn/TiO_2**, (B) **10%Zn/TiO_2**, and (C) **10%Zn/TiO_2** after annealing at 1000 °C for 10 h.

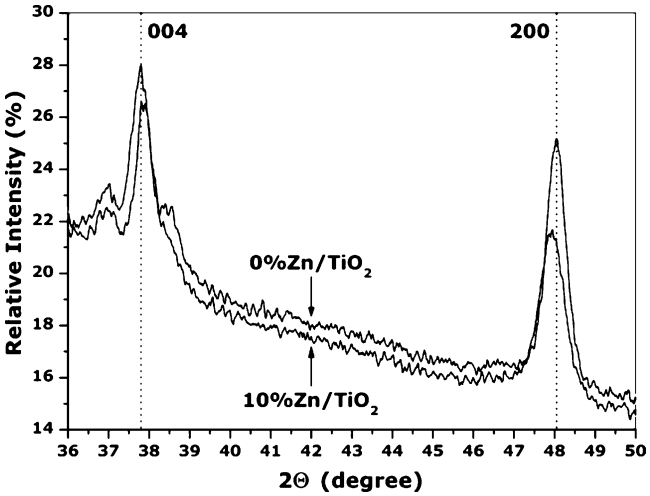

Figure 3. Comparison of the positions of the diffraction maxima 004 and 200 for anatase diffraction patterns of **0%Zn/TiO_2** and **10%Zn/TiO_2** samples.

undoped TiO_2. The decrease in particle size may be attributed to an increase of the Zn–O–Ti bonds in the doped samples, which inhibits a growth of the crystal grains.[19] It should be noted that the XRD patterns of all samples are very similar and peaks related to the presence of separate Zn-containing phases were not detected (parts A and B of Figure 2).

A different result is obtained after annealing the sample **10%Zn/TiO_2** at 1000 °C for 10 h. According to the XRD analysis (Figure 2C), this sample is a mixture of rutile (JCPDS no. 21-1276) and Zn_2TiO_4 (JCPDS no. 25-1164), that is, under thermal annealing of **10%Zn/TiO_2** at 1000 °C, the anatase phase transforms to rutile and the interaction between titania and the Zn-containing phase results in the formation of Zn_2TiO_4.

There are three possible locations for the Zn in the nanocomposite samples: in a separate amorphous phase, adsorbed on the surface of titania, or incorporated in the structure of the titania (partial substitution of Ti by Zn). The latter possibility can be tested by careful analysis of XRD data. First, we compare the theoretical patterns of pure anatase and hypothetical anatase, where 10% of titanium atoms are substituted by zinc atoms. Negligible changes in peak intensities are observed. Then we calculate the anatase unit cell parameters for all synthesized samples. It should be noted, that all samples are nanopowders, hence the quality of diffraction patterns is quite low (very broad peaks and high background). Another problem that hampers a precise determination of the unit cell parameters is the low number of well-defined diffraction maxima. Only 12 reflections of anatase were used in the refinement, and taking into account the tetragonal symmetry of anatase, this leads to a data/parameter ratio of only 6. To improve the accuracy of the unit cell parameter determination, an internal standard LaB_6 (cubic, a = 4.15692 Å) was used. For all samples, the calculated unit cell parameters a and c and unit cell volume V differ not more than 3σ, where σ is the standard deviation. For example, for the sample **0%Zn/TiO_2**, we obtained a = 3.7861(5) Å, c = 9.509(2) Å, V = 136.31(7) $Å^3$, while for the sample **10%Zn/TiO_2**, we obtained a = 3.792(2) Å, c = 9.493(4) Å, V = 136.5(2) $Å^3$. The ionic radius of Zn^{2+} in an octahedral environment is 0.73 Å, while the ionic radius of Ti^{4+} in an octahedral environment is 0.61 Å,[20] and an increase of the unit cell volume is expected.

Despite the very small differences in unit cell parameters, it can be speculated that the tetragonal parameter a slightly increases and the tetragonal parameter c slightly decreases with increasing Zn content. This is demonstrated in Figure 3 where the 004 and 200 diffraction peaks of anatase are shown for the **0%Zn/TiO_2** and **10%Zn/TiO_2** samples. In the **10%Zn/TiO_2** sample, the 004 peak is shifted to higher 2θ angles, while the 200 peak is shifted to smaller 2θ angles compared to the **0%Zn/TiO_2** sample. There are two examples of mixed Zn–Ti oxides described in the literature where zinc atoms have an octahedral environment. In the compound $ZnTiO_3$, zinc and titanium atoms occupy separate crystallographic positions, both of them have an octahedral oxygen coordination, but the ZnO_6 octahedron is more distorted than the TiO_6 one (Ti–O bonds, 2.01 Å × 3, 2.06 Å × 3; Zn–O bonds, 2.15 Å × 3; 2.95 Å × 3).[21] In the second compound, Zn_2TiO_4 spinel, half of the zinc atoms

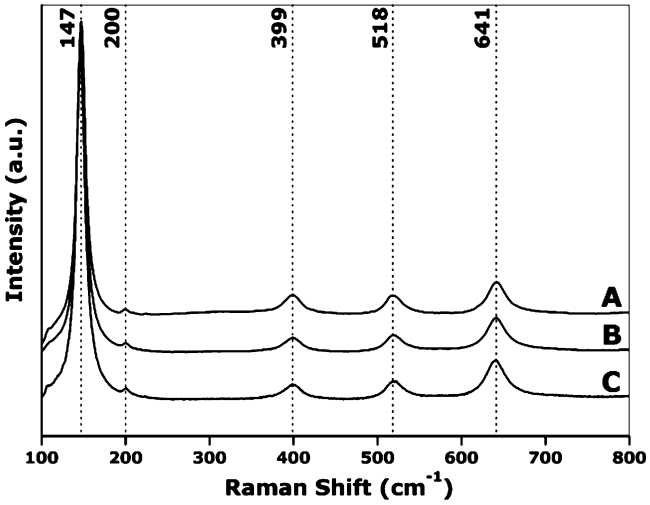

Figure 4. Raman spectra of samples **0%Zn/TiO$_2$** (A), **5%Zn/TiO$_2$** (B), and **10%Zn/TiO$_2$** (C).

together with the titanium atoms occupy octahedral positions; consequently, the Ti−O and Zn−O distances are the same, 2.02 Å.[21] The formation of a solid solution based on the anatase structure with an increase of the unit cell volume is possible, and the incorporation of Zn atoms in the structure of anatase should result in small distortions of the MO_6 octahedra; these may lead to the observed changes in unit cell parameters. However, these changes are very small, and the possible incorporation of Zn into the crystal structure of anatase needs additional proof.

To further understand where the doped Zn^{2+} cations are located, the synthesized Zn/TiO_2 nanocomposites are characterized by Raman spectroscopy, TEM, and ED techniques.

The fact that no zinc oxide phase has been detected by XRD could be related to an ill-crystallized ZnO, uniformly adsorbed on the surface of TiO_2. It should be emphasized that the zinc-containing samples were prepared by supercritical drying at 300 °C for 1 h followed by calcination at 500 °C for 10 h which is sufficient for the formation of crystalline ZnO.[22]

This possibility of a surface modification of TiO_2 by ZnO has been monitored by Raman spectroscopy. Figure 4 shows a typical Raman spectrum of a pure titania and powders of **5%Zn/TiO$_2$** and **10%Zn/TiO$_2$**. The Raman lines at 147, 200, 399, 518, and 641 cm^{-1} can be assigned to the $E_{g(1)}$, $E_{g(2)}$ $B_{1g(1)}$, A_{1g} + $B_{1g(2)}$, and $E_{g(3)}$ modes of the TiO_2 anatase phase, respectively.[23] It should be noted that no modes of ZnO or another Zn-containing phase have been detected in Raman spectra of samples **5%Zn/TiO$_2$** and **10%Zn/TiO$_2$** (parts B and C of Figure 4).[24] Mallick et al. have shown[25] that covering of the titania surface by ZnO results in drastic changes in the intensity of the Raman peaks. It was most pronounced for the peak at 147 cm^{-1}.[25] In our case, there are practically no changes in the intensity of the Raman peaks which indicate that surface modification of TiO_2 by ZnO has not taken place. Zn/TiO_2 nanocomposites keep the overall crystal structure of the TiO_2 anatase phase.

A correlation between the Raman peak width and the particle size was analyzed as a characteristic feature of the Raman spectra of the powders.[23b] In Table 1, data on the line width (fwhm) for the $E_{g(1)}$ mode are presented. In earlier work, Swamy et al.[23b] proposed the q vector relaxation model for phonon confinement behavior in anatase nanocrystals. We should mention here that in our work a good agreement between fwhm, particle size, and the phonon confinement model was observed.

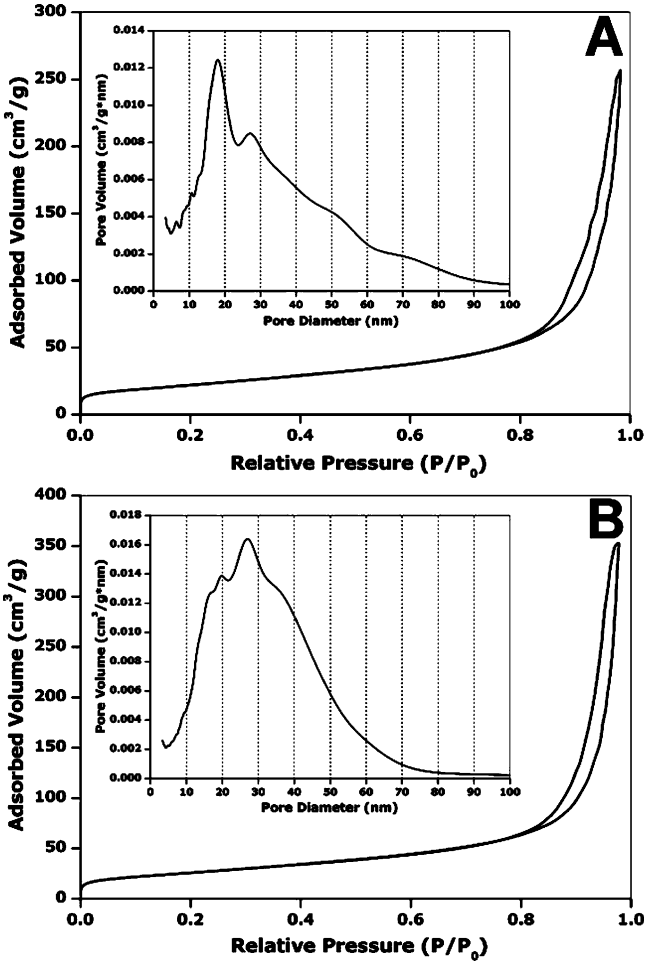

Figure 5. N_2 adsorption−desorption isotherms and pore size distribution (inset) of samples **0%Zn/TiO$_2$** (A) and **5%Zn/TiO$_2$** (B).

It was found that the size of the anatase crystallites should decrease from ∼15 to ∼11.5 nm by the phonon confinement model with an increase of the fwhm from 11.26 (sample **0%Zn/TiO$_2$**) to 12.27 cm^{-1} (sample **10%Zn/TiO$_2$**);[23b] this agrees well with the line-broadening analysis for these materials (Table 1).

Figure 5 shows the nitrogen adsorption and desorption isotherms and pore size distribution curves of **0%Zn/TiO$_2$** and **5%Zn/TiO$_2$** powders. It should be noted that the isotherms of all synthesized samples are quite similar and according to IUPAC classification, these isotherm shapes are of type IV.[26] The isotherms of both samples show a hysteresis at a relative pressure above $P/P_0 = 0.4$, associated with capillary condensation in the mesopores range. The hysteresis loops have an upward curvature at a relative pressure above 0.8. This upward curvature indicates the presence of cylindrical mesopores.[27] The comparison of pore size distribution (insets in Figure 5) for these two samples indicates that, in the case of pure TiO_2 powder, there are relatively large mesopores with a size of ∼18 nm, while in the case of the powder with 5.0 mol % Zn, a mesopore system with pores of ∼27 nm diameter is formed, that is, we have the formation of a new nanocomposite with different properties than pure mesoporous anatase. Moreover, the porosity of the obtained powders increases with increasing zinc content and the mesopores are better ordered.

In Table 1, the representative data of the BET surface area and the mesopore volumes of all synthesized are given. The pure TiO_2 powder has a high specific surface area (77 m^2/g) and a total mesopore volume (0.38 cm^3/g), which increases up to 94 m^2/g and 0.74 cm^3/g, respectively, for the powder with

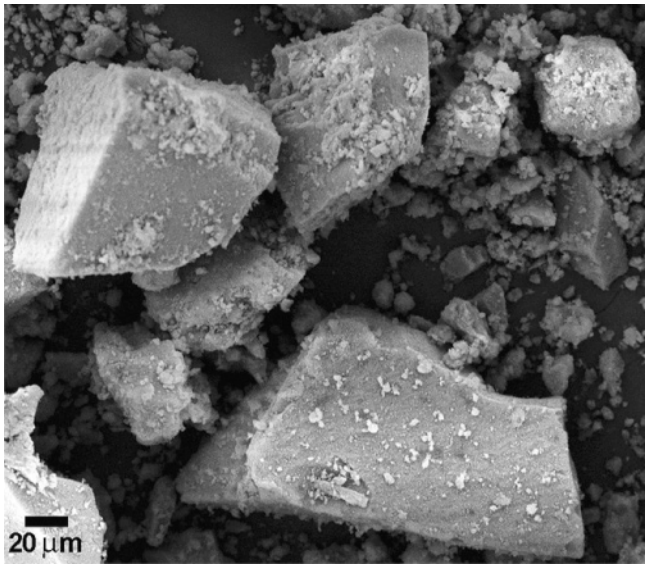

Figure 6. SEM microphotograph of the **5%Zn/TiO₂** nanocomposite prepared by the sol-gel method followed by supercritical drying.

10.0 mol % Zn. But, at the same time, there is no significant increase of the specific surface area for the samples containing a considerable amount of Zn (5.0, 10.0 mol %), that is, prepared samples possess a high crystallinity and there is no amorphous zinc-containing phases in the prepared samples.

SEM images of the sample **5%Zn/TiO**$_2$ show the typical morphology of the prepared powders (Figure 6). Supercritical drying of titania alcogels containing 5.0 mol % of zinc leads to the formation of small and mostly relatively big aggregates, consisting of sharp faceted nanoscaled crystals with a mean particle size of ~15 nm (TEM, Figure 7A). No significant differences are observed when comparing the morphology of the synthesized samples.

Electron diffraction of the **5%Zn/TiO**$_2$ sample shows a distinct ring pattern, typical for nanoparticle clustering (Figure 7B). The rings of the ED pattern can be completely indexed in the anatase tetragonal I_1/amd space group, using the anatase unit cell parameters of JCPDS no. 21-1272. A calculated electron diffraction pattern (inset in Figure 7B) for TiO_2 is in good agreement with the experimental image and corresponds to the anatase structure. No rings corresponding to a secondary phase or to an amorphous phase are present.

To understand the microstructure of the sample with a Zn content of 5.0 mol %, HRTEM (high-resolution transmission electron microscopy) measurements were carried out. Figure 8 shows HRTEM images of single anatase nanoparticles along the [111] and [100] zone axes. The corresponding Fourier transform patterns of the single anatase nanoparticles are shown as an inset. These patterns can be indexed according to the anatase structure. The individual nanoparticles are highly crystalline and defect free. The calculated images, using the crystal parameters of anatase, for different defocus values and thickness are in good agreement with the experimental images. One of them is included as an inset for each nanoparticle. The edges of the particles are well defined, sharp, and free of any amorphous or secondary phase at the surface. Possible distortions are not observed, that is, if they are present, then they are very small and for a particle size of 10−20 nm, without internal calibration, difficult to detect.

Although no amorphous phase or other crystalline phases are detected in the **5%Zn/TiO**$_2$ sample, EDX taken from selected areas (including several nanoparticles) shows the presence of zinc in the sample.

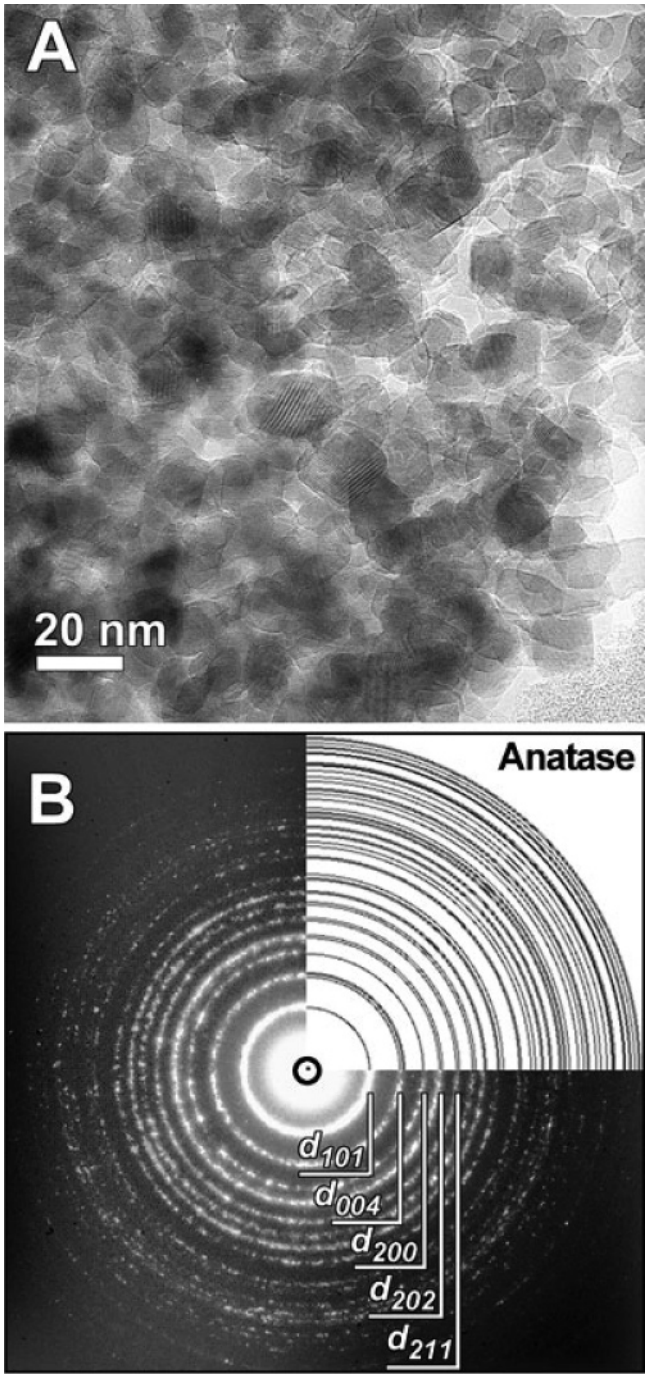

Figure 7. Low-magnification TEM image (A) and corresponding electron microdiffraction pattern (B) of a **5%Zn/TiO₂** nanocomposite prepared by the sol-gel method followed by supercritical drying. The calculated powder electron diffraction pattern (FFT) is shown as an inset in Figure 7B.

The line-broadening analysis of the crystalline size (Table 1) is in good agreement with the data obtained directly by TEM. The particles should therefore be considered as single domains. Owing to N_2 adsorption−desorption and TEM results, the mesoporous structure of prepared powders can be attributed to the random agglomeration of anatase nanocrystals which leads to the formation of a disordered porous system in the mesopore-sized region.[28]

The influence of Zn on the electronic structure of the Zn/TiO_2 nanocomposites can be also examined in the band-gap energy. Figure 9A shows the UV−vis spectra of as-prepared powders (samples **0%Zn/TiO**$_2$, **0.5%Zn/TiO**$_2$, and **5%Zn/**

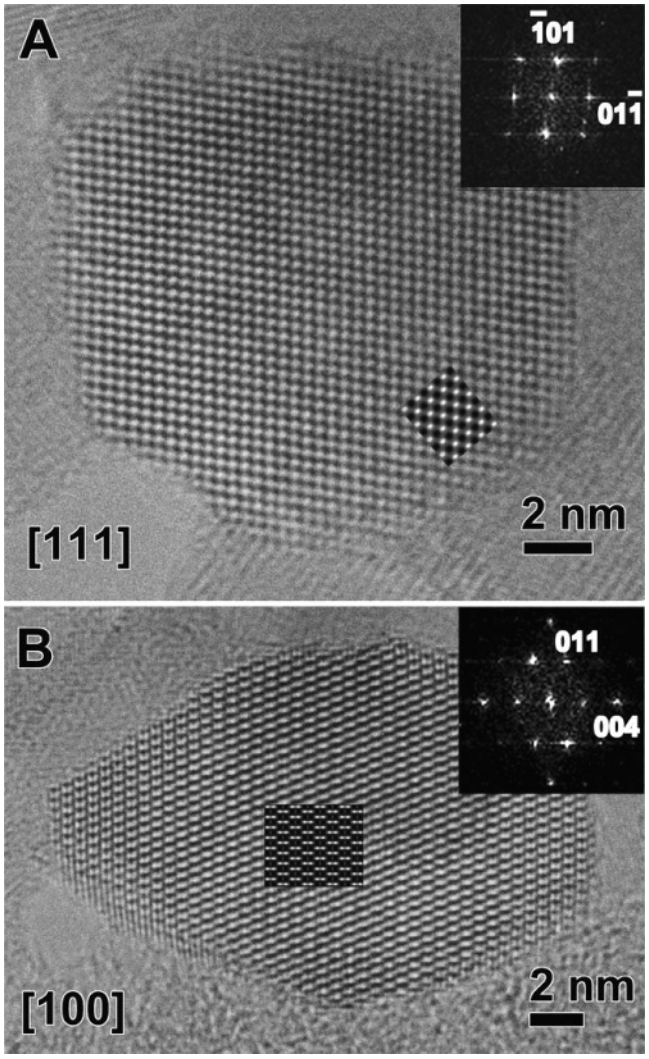

Figure 8. High-resolution electron microscopy image along [111] (A) and [100] (B) of the lamellar single anatase particles (sample **5%Zn/TiO$_2$**). The calculated electron diffraction patterns (FFT) and simulated images (A, defocus of −400 Å, thickness of 40 Å and B, defocus of −200 Å, thickness of 80 Å) are shown as insets.

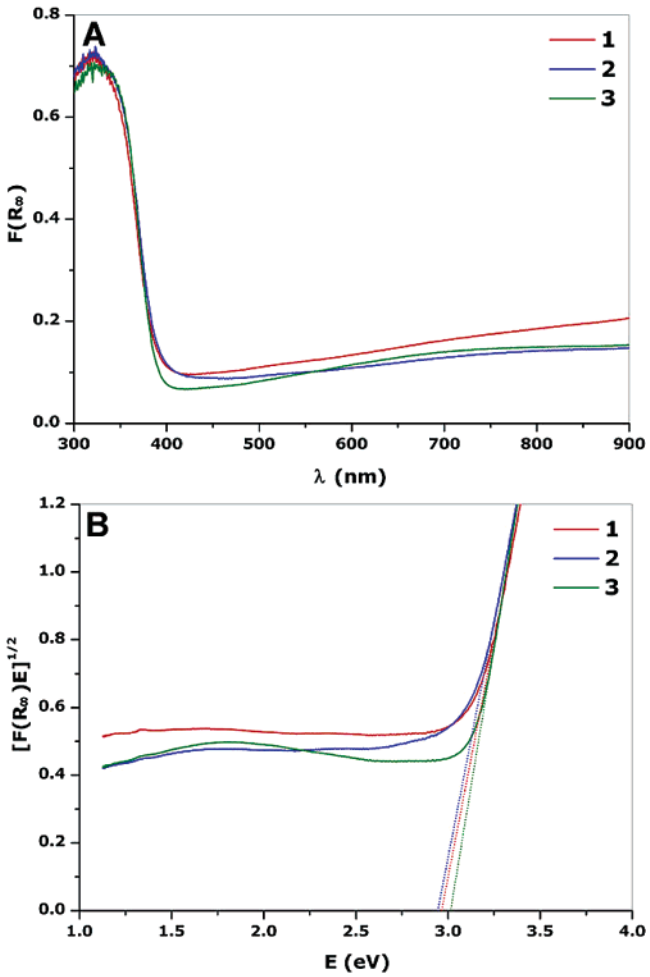

Figure 9. Diffuse reflectance spectra (A) and a plot of the transformed Kubelka−Munk function vs the energy of the light absorbed (B) of TiO_2 and Zn/TiO_2 powders synthesized by the sol-gel method followed by supercritical drying: (1) **0%Zn/TiO$_2$**, (2) **0.5%Zn/TiO$_2$**, and (3) **5%Zn/TiO$_2$**.

TiO$_2$) with a different zinc ratio. A plot of the modified Kubelka−Munk function vs the energy of the exciting light (Figure 9B)[29] gives the band-gap energies at room temperature in Table 1 assuming that materials such as TiO_2 are indirect conductors. Generally, bulk anatase is a semiconductor with a band-gap energy of 3.23 eV, corresponding to light with a wavelength λ of 385 nm.[30] The band gap of the synthesized pure anatase powder (sample **0%Zn/TiO$_2$**) as calculated from the extrapolation of the absorption edge onto the energy axis is 2.96 eV ($\Delta E_{bg} \sim 0.27$ eV). The sizable red shift in the band gap can be due to the lattice strain in the nanosized anatase particles[31] and/or a direct transition in the otherwise indirect band-gap semiconductor.[32] The absorption of pure titania in the visible light region is less intensive than that for the Zn/TiO_2 nanocomposites (Figure 9A).[33] The diffuse reflectance spectra of the zinc-containing powders show a blue shift in the band-gap energy, depending on the concentration of the dopant (Table 1, Figure 9B). This observation may be connected with a decrease in the particle size (Table 1) and the incorporation of metal ions.[8a] It should be noted that additional band edges (doping absorption edge and/or pure ZnO edge at 3.37 eV) have not been found in diffuse reflectance spectra, that is, the formation of ZnO phases does not take place.

By summarizing the results of all used characterization techniques, we are able to make a conclusion concerning the nature of zinc in synthesized samples. Chemical analysis and EDX show zinc's presence in our samples, moreover, EDX shows a very homogeneous distribution of the zinc over the samples. On the X-ray diffraction patterns of all synthesized samples, only anatase peaks are detected, meaning no another crystalline phase is formed; however, according to the XRD pattern, sample **10%Zn/TiO$_2$** annealed at 1100 °C is a mixture of rutile and Zn_2TiO_4. Small changes in the unit cell parameters with increasing zinc content are detected. Raman spectra also show only modes belonging to anatase, proving that no other amorphous phase or surface phase is formed. BET and TEM as well show the absence of an amorphous zinc-containing phase—no significant increase of the surface area for samples with high zinc content was detected. UV−vis spectroscopy shows small changes in adsorption spectra of samples with different zinc content, but all spectra are similar to one of pure anatase. According to TEM, only one type of particle is present in the samples and ED patterns of the particles are in good agreement with the anatase structure; finally, HREM clearly shows the absence of any type of defect, antiphase boundaries, or clusters in the nanoparticles structure. The calculated images for the anatase structure agree well with the observed ones. A comparison of the data of all methods may demonstrate that, in the synthesized samples, zinc does not form a separate

crystalline or amorphous phase but fully dissolves in the anatase lattice. The intercalation of Li ions to pores of the anatase crystal structure is known,[34] but the Zn^{2+} ion has a significantly larger radius than the Li^+ ion, moreover, such an intercalation should be clearly seen on the HREM images. Apparently, in the case of our samples, another possibility is realized and the solid solution $Zn_xTi_{1-x}O_{2-x}$ (x from 0 to 0.1) is formed. As was mentioned above, there is an example of a mixed occupancy of the octahedral position by both zinc and titanium atoms in the spinel Zn_2TiO_4. Also, the formation of the wide-range solid solution ZnO/TiO_2 based on another modification of titania−srilankite was reported.[35] An additional reason for solid solution stabilization may be the finite size of the particles ~15 nm. Such a small size of crystallites also makes it very difficult for precise investigations of the unit cell parameters, that is why we cannot prove the formation of $Zn_xTi_{1-x}O_{2-x}$ solid solution by standard XRD techniques (validation of Vegard's law).

Our preliminary investigation shows that synthesized samples exhibit significant photocatalytic activity in the reaction of phenol photodegradation, also a strong influence of zinc content on photocatalytic activity was detected. We will continue the investigations of the photocatalytic properties of the title solid solution.

Conclusion

We have investigated the formation and properties of mixed Zn/Ti oxides prepared by a template-free sol-gel method followed by high-temperature supercritical drying in 2-propanol. Mesoporous anatase particles are formed with a particle size between 13 and 17 nm. A detailed investigation of the samples with a set of methods (XRD, SEM, TEM, ED, HREM, EDX, ICP-OES, N_2 adsorption−desorption, Raman spectroscopy, and UV−vis spectroscopy) shows that zinc does not form as a separate crystalline or amorphous phase but fully dissolves in the anatase lattice, apparently forming a solid solution $Zn_xTi_{1-x}O_{2-x}$. The photocatalytic activity of synthesized materials is currently under investigation.

Acknowledgment. We are grateful to Mrs. U. Schmidt and Dr. G. Auffermann for the chemical analysis, Dr. H. Borrmann for collecting the XRD data, Dr. A.V. Olenev for EDX analysis, and Mrs. M.Yu. Kustova for elaboration of the BJH results. The work is supported by the Russian Foundation for Basic Research, Grant No. 04-03-32295 and No. 05-03-33036. The authors gratefully acknowledge support from the "Rosnauka" under the project IN-12.5/002. K.A.K. thanks the Max-Plank Society for research fellowship and Yu.V.K. thanks the FY2005 JSPS Postdoctoral Fellowships for Foreign Researchers.

References and Notes

(1) (a) Harris, D. *Annual Report Kronos International*; 1996; p 104. (b) Hewitt, J. *Cosmet. Toiletries* **1999**, *114*, 59. (c) Pillips, L. G.; Barbano, D. M. *J. Dairy Sci.* **1997**, *80*, 2726.

(2) Diebold, U. *Surf. Sci. Rep.* **2003**, *48*, 53.

(3) (a) Guidi, V.; Carrota, M. C.; Ferroni, M.; Martinelli, G. *Sens. Actuators, B* **1999**, *57*, 197. (b) Devi, G. S.; Hyodo, T.; Shimizu, Y.; Egashira, M. *Sens. Actuators, B* **2002**, *87*, 122.

(4) (a) Nakade, S.; Kanzaki, T.; Kubo, W.; Kitamura, T.; Wada, Y.; Yanagida, S. *J. Phys. Chem. B* **2005**, *109*, 3480. (b) Nakade, S.; Makimoto, Y.; Kubo, W.; Kitamura, T.; Wada, Y.; Yanagida, S. *J. Phys. Chem. B* **2005**, *109*, 3488. (c) Kitamura, T.; Ikeda, M.; Shigaki, K.; Inoue, T.; Anderson, N. A.; Ai, X.; Lian, T.; Yanagida, S. *Chem. Mater.* **2004**, *16*, 1806. (d) Ito, S.; Takeuchi, T.; Katayama, T.; Sugiyama, M.; Matsuda, M.; Kitamura, T.; Wada, Y.; Yanagida, S. *Chem. Mater.* **2003**, *15*, 2824.

(5) (a) Sambrano, J. R.; Andres, J.; Beltran, A.; Sensato, F. R.; Leite, E. R.; Stamato, F. M. L. G.; Longo, E. *Int. J. Quantum Chem.* **1997**, *65*, 625. (b) Chambers, S. A.; Thevuthasan, S.; Farrow, R. F. C.; Marks, R. F.; Thiele, J. U.; Folks, L.; Samant, M. G.; Kellock, A. J.; Ruzycki, N.; Ederer, D. L.; Diebold, U. *Appl. Phys. Lett.* **2001**, *79*, 3467. (c) Matsumoto, Y.; Murakami, M.; Shono, T.; Hasegawa, T.; Fukumura, T.; Kawasaki, M.; Ahmet, P.; Chikyow, T.; Koshihara, S.; Koinuma, H. *Science* **2001**, *291*, 854. (d) Bonhote, P.; Gogniat, E.; Gratzel, M.; Ashrit, P. V. *Thin Solid Films* **1999**, *350*, 269.

(6) (a) Sittig, C.; Textor, M.; Spencer, N. D.; Wieland, M.; Vallotton, P. H. *J. Mater. Sci.: Mater. Med.* **1999**, *10*, 35. (b) Lausmaa, J.; Ask, M.; Rolander, U.; Kasemo, B. *Mater. Res. Soc. Symp. Proc.* **1989**, *110*, 647.

(7) Kamat, P. V. In *Semiconductor Nanoclusters-Physical, Chemical and Catalytic aspects*; Kamat, P. V.; Meisel, D., Eds.; Elsevier Science: Amsterdam, The Netherlands, 1997; p 237.

(8) (a) Carp, O.; Huisman, C. L.; Reller, A. *Prog. Solid State Chem.* **2004**, *32*, 33. (b) Irie, H.; Sunada, K.; Hashimoto, K. *Electrochemistry* **2004**, *72*, 807.

(9) Cao, Y. A.; Yang, W. S.; Zhang, W. F.; Liu, G. Z.; Yue, P. L. *New J. Chem.* **2004**, *28*, 218.

(10) Haick, H.; Paz, Y. *J. Phys. Chem. B* **2003**, *107*, 2319.

(11) (a) Chan, S. C.; Barteau, M. A. *Langmuir* **2005**, *21*, 5588. (b) Wang, X.; Yu, J. C.; Yip, H. Y.; Wu, L.; Wong, P. K.; Lai, S. Y. *Chem.−Eur. J.* **2005**, *11*, 2997. (c) Kumar, A.; Mathur, N. *Appl. Catal., A* **2004**, *275*, 189. (d) Zafeiratos, S., Papakonstantinou, G., Jacksic, M. M., Neophytides, S. G. *J. Catal.* **2005**, *232*, 127. (e) Yang, J. H.; Henao, J. D.; Raphulu, M. C.; Wang, Y.; Caputo, T.; Groszek, A. J.; Kung, M. C.; Scurrell, M. S.; Miller, J. T.; Kung, H. H. *J. Phys. Chem. B* **2005**, *109*, 10319.

(12) Al-Salim, N. Y.; Abagshaw, S.; Bittar, A.; Kemmett, T.; McQuilla, A. J.; Mills A. M.; Ryan, M. J. *J. Mater. Chem.* **2000**, *10*, 2358. (b) Xu, A. W.; Gao, Y.; Xu, H. Q. *J. Catal.* **2002**, *207*, 151.

(13) (a) Choi, W.; Termin, A.; Hoffmannn, M. R. *Angew. Chem., Int. Ed.* **1994**, *33*, 1091. (b) Choi, W.; Termin, A.; Hoffmannn, M. R. *J. Phys. Chem.* **1994**, *98*, 13669.

(14) (a) Gennari, F. C.; Pasquevich, D. M. *J. Mater. Sci.* **1998**, *33*, 1571. (b) Bally, A. R.; Korobeinikova, E. N.; Schmid, P. E.; Levi, F.; Bussy, F. *J. Phys. D: Appl. Phys.* **1998**, *31*, 1149.

(15) (a) Borgarello, E.; Kiwi, J.; Gratzel, M., Pelizzetti, E.; Visca, M. *J. Am. Chem. Soc.* **1982**, *104*, 2996. (b) Navio, J. A.; Colon, G.; Litter, M. I.; Bianco G. N. *J. Mol. Catal. A: Chem.* **1996**, *16*, 267.

(16) (a) Pierre, A. C. *Introduction to Sol-Gel Processing*; Kluwer Academic Publishers: Boston, MA, 1998; chapter 1. (b) Schneider, M.; Baiker, A. *Catal. Today* **1997**, *35*, 339. (c) Pierre, A. C.; Pajonk, G. M. *Chem. Rev.* **2002**, *102*, 4243.

(17) Schneider, M.; Baiker, A. *Catal. Rev. − Sci. Eng.* **1995**, *37*, 515.

(18) Dagan, G.; Tomkiewicz, M. *J. Phys. Chem.* **1993**, *97*, 12651.

(19) Lin, J.; Yu, J. C. *J. Photochem. Photobiol., A.* **1998**, *116*, 63.

(20) (a) Shannon R. D.; Prewitt C. T. *Acta Crystallogr.* **1969,** *B25*, 925. (b) Shannon R. D. *Acta Crystallogr.* **1976**, *A32*, 751.

(21) Bartram, S. F.; Slepetys, R. A. *J. Am. Ceram. Soc.* **1961**, *44*, 493.

(22) (a) Armelao, L.; Fabrizio, M.; Gialanella, S.; Zordan, F. *Thin Solid Films* **2001**, *394*, 90. (b) Cannas, C.; Mainas, M.; Musinu, A.; Piccaluga, G. *Compos. Sci. Technol.* **2003**, *63*, 1187.

(23) (a) Balachandran, U.; Eror, N. G. *J. Solid State Chem.* **1982**, *42*, 276. (b) Swamy, V.; Kuznetsov, A.; Dubrovinsky, L. S.; Caruso, R. A.; Shchukin, D. G.; Muddle, B. C. *Phys. Rev. B* **2005**, *71*, 184302.

(24) Xing, Y. J.; Xi, Z. H.; Xue, Z. Q.; Zhang, X. D.; Song, J. H.; Wang, R. M.; Xu, J.; Song, Y.; Zhang, S. L.; Yu, D. P. *Appl. Phys. Lett.* **2003**, *83*, 1689.

(25) Mallick, K.; Scurrell, M. S. *Appl. Catal., A* **2003**, *253*, 527.

(26) Thomas, J. M.; Thomas, W. J. *Principles and Practice of Heterogeneous Catalysis*; VCH Publishers Inc.: New York, 1997; p 80.

(27) Janssen, A. H.; Schmidt, I.; Jacobsen, C. J. H.; Koster, A. J.; de Jong, K. P. *Microporous Mesoporous Mater.* **2003**, *65*, 59.

(28) (a) Sreethawong, T.; Suzuki, Y.; Yoshikawa, S. *J. Solid State Chem.* **2005**, *178*, 329. (b) Huang, W.; Tang, X.; Wang, Y.; Koltypin, Y.; Gedanken, A. *Chem. Commun.* **2000**, 1415. (c) O'Regan, B.; Gratzel, M. *Nature* **1991**, *353*, 737. (d) Bach, U.; Lupo, D.; Comte, P.; Moser, J. E.; Weissortel, F.; Salbeck, J.; Spreitzer, H.; Gratzel, M. *Nature* **1998**, *395*, 583.

(29) Kubelka, P. *J. Opt. Soc. Am.* **1948**, *38* (5), 448.

(30) Judin, V. S. P. *Chem. Br.* **1993**, 503.

(31) Vassiliou, J. K.; Mehrotra, V.; Russell, M. W.; Giannelis, E. P. *J. Appl. Phys.* **1993**, *73*, 5109.

(32) (a) Serpone, N.; Lawless, D.; Khairutdinov, V. *J. Phys. Chem.* **1995**, *98*, 16646. (b) Reddy, K. M.; Mamorama, S. V.; Reddy, A. M. *Mater. Chem. Phys.* **2002**, *78*, 239.

(33) Sreethawong, T.; Ngamsinlapasathian, S.; Suzuki, Y.; Yoshikawa, S. *J. Mol. Catal. A: Chem.* **2005**, *235*, 1.

(34) (a) Wagemaker, M.; van Well, A. A.; Kearley, G. J.; Mulder F. M. *Solid State Ionics* **2004**, *175*, 191. (b) Smirnov, M.; Baddour-Hadjean, R. *J. Chem. Phys.* **2004**, *121*, 2348. (c) Koudriachova, M. V.; de Leeuw, S. W.; Harrison, N. M. *Phys. Rev. B.* **2004**, *69*, 054106.

(35) Manik, S. K.; Bose, P.; Pradhan, S. K. *Mater. Chem. Phys.* **2003**, *82*, 837.